

# Elimination, reversal and directional bias of optical diffraction

Ofer Firstenberg<sup>1\*</sup>, Paz London<sup>1</sup>, Moshe Shuker<sup>1</sup>, Amiram Ron<sup>1</sup> and Nir Davidson<sup>2</sup>

**Any image, imprinted on a wave field and propagating in free space, undergoes a paraxial diffraction spreading. The reduction or manipulation of diffraction is desirable for many applications, such as imaging, wave-guiding, microlithography and optical data processing. As was recently demonstrated, arbitrary images imprinted on light pulses are dramatically slowed<sup>1,2</sup> when traversing an atomic medium of electromagnetically induced transparency<sup>3,4</sup> and undergo diffusion due to the thermal atomic motion<sup>5,6</sup>. Here we experimentally demonstrate a new technique to eliminate the paraxial diffraction and the diffusion of slow light, regardless of its position and shape<sup>7</sup>. Unlike former suggestions for diffraction manipulation<sup>8–12</sup>, our scheme is linear and operates in the wavevector space, eliminating the diffraction for arbitrary images throughout their propagation. By tuning the interaction, we further demonstrate acceleration of diffraction, biased diffraction and induced deflection, and reverse diffraction, implementing a negative-diffraction lens<sup>13</sup>. Alongside recent advances in slow-light amplification<sup>14</sup> and image entanglement<sup>15</sup>, diffraction control opens various possibilities for classical and quantum image manipulation.**

Electromagnetically induced transparency (EIT) is a coherent two-photon interaction between light and atoms<sup>16</sup>. It involves an atomic medium and two light fields, usually a strong ‘pump’ and a weak ‘probe’, resonantly coupling two of the atomic levels to a common excited level. When the Raman resonance condition is satisfied, namely when the two-photon frequency detuning,  $\Delta$ , is within the atomic spectral width,  $\Gamma$ , the atoms are driven towards a ‘dark’ state, which substantially reduces the absorption in the medium. A short probe pulse propagates in the medium with a reduced group velocity, owing to the steep dispersion inside the narrow transparency window<sup>4,17–21</sup>. A travelling atomic-coherence field accompanies the probe, and the combined light-matter excitation is termed a dark-state polariton<sup>22</sup>. If an image is imprinted on the probe field in the plane normal to the propagation direction, the complex amplitude of the dark-state polariton follows the amplitude and phase of the image. Free-space diffraction, being essentially a geometric effect, occurs for slow images precisely as it would in free space.

In an EIT medium of hot vapour, the thermal motion of the atoms affects the propagation of images. The addition of a buffer gas attenuates the thermal motion, which becomes diffusive and can be characterized by a single diffusion coefficient,  $D$ . As a result, on EIT resonance, the atomic part of the dark-state polariton undergoes diffusion while propagating slowly in the medium<sup>5</sup>. The polariton thus experiences both diffraction and diffusion. Here, we exploit the atomic motion to influence the diffraction, as illustrated in Supplementary Fig. S1. Altering the Raman detuning provides control of the polariton’s coupling with atoms moving

in a desired direction. We therefore counterbalance diffraction by ‘Doppler trapping’ the outwards-confronting light components with inwards-moving atoms or, alternatively, force diffraction in a preferable direction.

The free-space diffraction of an optical field envelope  $E(x, y; z)$  travelling in the  $z$  direction is described in the transverse Fourier plane (Fig. 1a) as  $\partial E(\mathbf{k}_\perp; z)/\partial z = [-ik^2/(2q)]E(\mathbf{k}_\perp; z)$ , where  $k = |\mathbf{k}_\perp|$  is the transverse wavenumber,  $q = 2\pi/\lambda$  and  $\lambda$  is the optical wavelength. In a vapour EIT medium, the propagation of a weak probe depends on its angular deviation from the pump due to the Doppler–Dicke effect<sup>23,24</sup>. For a wide homogenous non-diverging pump, finite-pump effects such as transverse intensity variation<sup>25</sup> and Ramsey narrowing<sup>26</sup> are made negligible, and the dynamics of the probe becomes<sup>5</sup>  $\partial E(\mathbf{k}_\perp; z)/\partial z = i\chi(\mathbf{k}_\perp)E(\mathbf{k}_\perp; z)$ , where  $\chi(\mathbf{k}_\perp) = \chi_{\text{EIT}}(\mathbf{k}_\perp) - k^2/(2q)$  is the linear susceptibility and

$$\chi_{\text{EIT}}(\mathbf{k}_\perp) = i\alpha \left( 1 - \frac{\Gamma_p}{\Gamma + Dk^2 - i\Delta} \right) \quad (1)$$

Here,  $2\alpha$  is the absorption outside the EIT window,  $\Gamma_p$  is the power-broadening width, proportional to the pump intensity, and  $Dk^2$  is the Doppler–Dicke width. The latter has a simple physical interpretation: both the residual Doppler broadening and the Dicke narrowing are linear in  $k$ , which corresponds to the angle between the probe and pump, resulting in a combined quadratic effect<sup>24</sup>. At a given  $\Delta$ , different  $k$  components of a probe image experience different EIT spectra, and consequently the image is altered. When  $\Delta = 0$  (red lines in Fig. 1b),  $\chi_{\text{EIT}}$  is purely imaginary and induces a low-pass absorption filter in  $k$  space, with a half-width of  $k_0 = \sqrt{\Gamma/D}$ . For  $k \ll k_0$ , the filter is quadratic in  $k$  and corresponds to standard diffusion, accompanied by the free-space diffraction. To manipulate diffraction, a non-zero Raman detuning should be introduced. The case  $\Delta = \pm\Gamma$  is of special importance: in this case, the leading quadratic term becomes purely real, inducing diffraction without diffusion,

$$\chi_{\text{EIT}}(\mathbf{k}_\perp) = \chi_{\text{EIT}}(0) \mp \frac{Dk^2}{2v_g} + O(k^4) \quad \text{for} \quad \Delta = \pm\Gamma \quad (2)$$

with  $v_g = \Gamma^2/(\alpha\Gamma_p)$  being the slow group velocity. Here, the induced diffraction is continuous, in contrast to the diffraction manipulation explored in periodic systems<sup>27–29</sup>. When  $\Delta = -\Gamma$  the induced diffraction negates the free-space diffraction, and if  $v_g = Dq$  they are cancelled altogether. As demonstrated in Fig. 1b (black lines), for  $k \ll k_0$ , the susceptibility curves are flat and both diffraction and diffusion are eliminated. In contrast, when  $\Delta = +\Gamma$ , the induced and the free-space diffraction add together, increasing the overall diffraction. Note that for given  $D$  and  $q$

<sup>1</sup>Department of Physics, Technion—Israel Institute of Technology, Haifa 32000, Israel, <sup>2</sup>Department of Physics of Complex Systems, Weizmann Institute of Science, Rehovot 76100, Israel. \*e-mail: oferfir@tx.technion.ac.il.

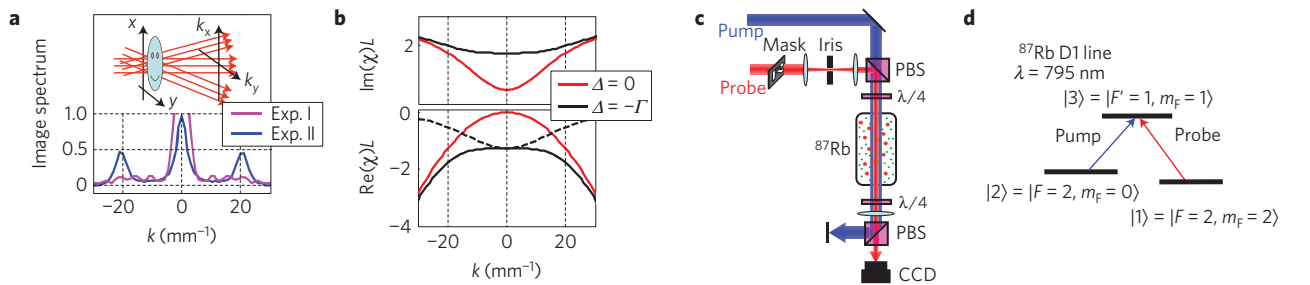


**Figure 1 | EIT susceptibility in  $k$  space and the experimental set-up.** **a**, An image in the transverse plane, decomposed into its transverse-momentum components. The spectra as a function of  $k$  correspond to the experiments presented in (I) Fig. 2a and (II) Fig. 2b. **b**, The total susceptibility (solid lines): imaginary part (top), corresponding to diffusion, and real part (bottom), corresponding to diffraction. For  $\Delta = -\Gamma$ , both curves are flat up to the fourth order in  $k$ . The dashed line shows the contribution from the EIT for  $\Delta = -\Gamma$ , imposing negative diffraction at  $k \ll k_0$  and cancelling the free-space diffraction ( $k_0 = 20 \text{ mm}^{-1}$ ). **c**, The experimental set-up. An image is imprinted on the probe beam using a binary mask, and is imaged onto the entrance facet of the cell by a  $4f$  imaging system. An iris in the central focus point acts as a low-pass filter for the image. The collimated pump and the probe, of orthogonal linear polarizations, are combined on a polarizing beam splitter (PBS), rotated to circular polarizations with a  $\lambda/4$  plate, passed through the 50-mm-long  $^{87}\text{Rb}$  cell, rotated back to linear polarizations and split using a second PBS. The probe is imaged from the exit facet of the cell onto a CCD (charge-coupled device) camera. Further details are given in Supplementary Information. **d**, The  $\Delta$ -type level diagram depicts the part of the  $^{87}\text{Rb}$  D1 line that was used in the experiment.

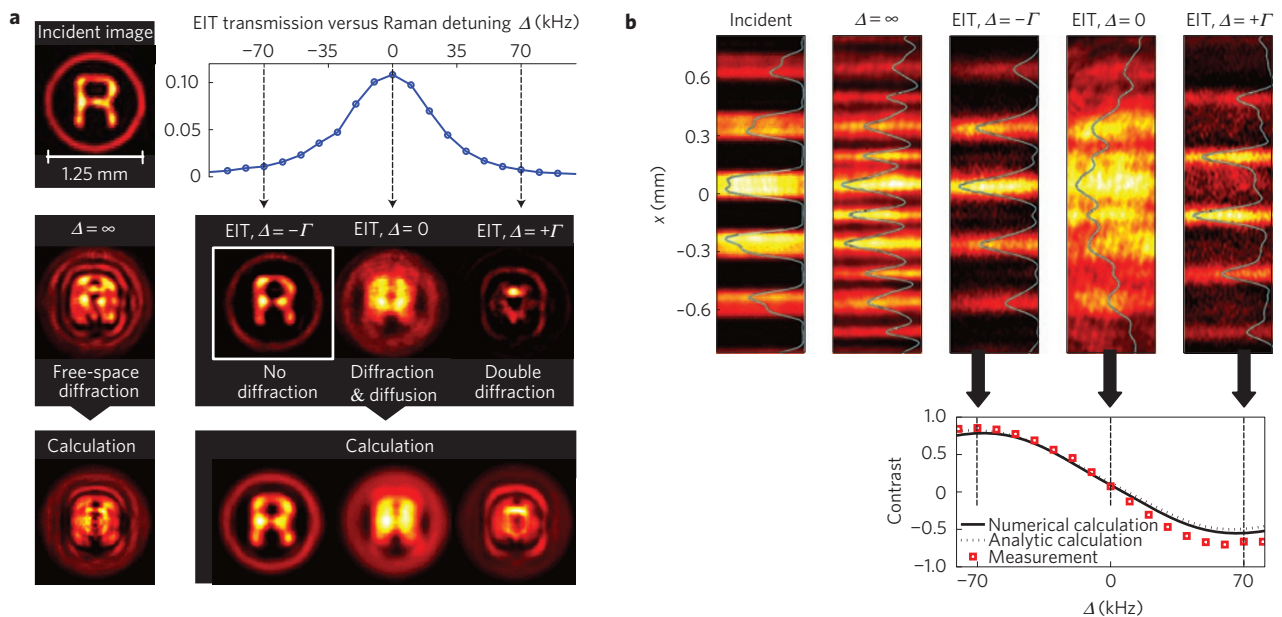


**Figure 2 | Elimination of diffraction of arbitrary images.** **a**, Top left, an image of the symbol ‘R’ at the entrance facet of the vapour cell. Middle row, the image at the exit facet of the 50 mm cell without EIT (left, taken at off-resonance) and with EIT (right), for  $\Delta = -\Gamma$ , 0, and  $+\Gamma$  ( $\Gamma = 70 \text{ kHz}$ ). The  $\Delta = 0$  image shows both the regular free-space diffraction and the diffusion associated with the atomic motion. The  $\Delta = -\Gamma$  image manifests the elimination of diffraction, as well as the absence of diffusion. The  $\Delta = +\Gamma$  image shows no diffusion and twice the effect of free-space diffraction—the sum of the free-space and the EIT-induced diffraction. The graph above indicates the transmitted power as a function of  $\Delta$ . Bottom row, numerical calculations of the effect for each case, given the initial condition of the incident image. The elimination of diffraction is insensitive to small changes in the experimental conditions—see Supplementary Fig. S3. **b**, The incident image is an array of lines ( $3.3 \text{ lp mm}^{-1}$ ), such that after 50 mm of free-space propagation ( $\Delta = \infty$ ) new lines appear in the dark centres between the original lines (a reciprocal grating at  $\sim 1/4$  Talbot distance, with  $L_T = 230 \text{ mm}$ ). The cyan curves are transverse cross-sections. The elimination of diffraction for  $\Delta = -\Gamma$  and the doubling of the diffraction for  $\Delta = +\Gamma$  are clearly seen. In the  $\Delta = +\Gamma$  image, the original grating almost vanishes, which is equivalent to a half Talbot distance. In the  $\Delta = 0$  image, regular free-space diffraction occurs (quarter Talbot distance), accompanied by diffusion, which completely blurs the lines. The bottom graph shows the contrast of the original grating compared to the reciprocal grating, with  $+1$  corresponding to the initial image and  $-1$  to the existence of only the reciprocal grating (half Talbot distance). The contrast is well explained by an analytic analysis, which considers the  $k$  spectrum of the image with a single carrier and two sidebands at  $\pm 2\pi/a$  (the exact spectrum is shown in Fig. 1a, Experiment II). The analytic expression is given in Supplementary Equation S5.

the amount of induced diffraction is determined exclusively by the group velocity, which is easily controlled by the pump power and the atomic density. A major difficulty of the scheme is the substantial absorption at  $\Delta \neq 0$ . Fortunately, this absorption is uniform both in real and  $k$  spaces and may be compensated for by any linear gain mechanism<sup>7,14</sup>.

The experimental set-up is depicted in Fig. 1c. A glass vapour cell of length  $L = 50 \text{ mm}$  is air-heated to  $72^\circ\text{C}$  and filled with  $^{87}\text{Rb}$  and 10 torr of neon buffer-gas. The rubidium diffusion coefficient is  $D = 1,100 \text{ mm}^2 \text{ s}^{-1}$ , satisfying the diffraction-elimination condition with  $v_g = Dq \approx 8,700 \text{ m s}^{-1}$ . For our optical depth ( $\sim 6$ ), we arrive at these conditions with a pump intensity of  $660 \mu\text{W mm}^{-2}$ , yielding

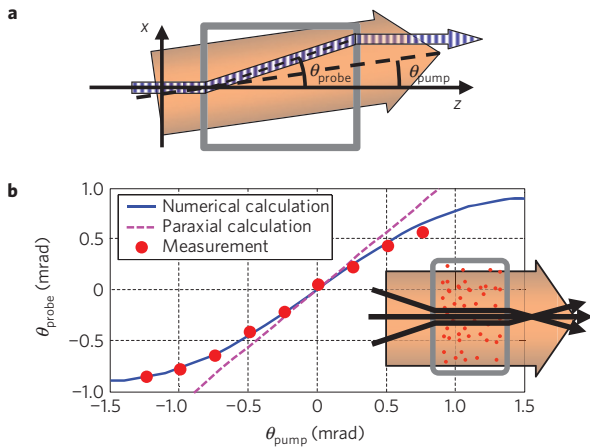


**Figure 3 | Induced deflection (walk-off) of the probe beam.** **a**, The pump is set at an angle  $\theta_{\text{pump}}$  relative to the  $z$  axis, and the angular deflection of the probe,  $\theta_{\text{probe}}$ , is measured. The drawing illustrates the directions for  $\Delta < 0$ . For  $\Delta > 0$ , the probe deflects in the opposite direction. **b**, At the conditions for diffraction elimination ( $\Delta = -\Gamma$ ,  $v_g = Dq$ ) the probe follows the direction of the pump for  $q\theta_{\text{pump}} \ll k_0$ . The experimental error in determining  $\theta_{\text{probe}}$  is  $\pm 0.02$  mrad; the error in  $\theta_{\text{pump}}$  is much smaller. Inset, An explanation of the diffraction elimination through the deflection effect. At these specific conditions, the probe beam ‘finds’ the pump and refracts in its direction, regardless of the probe’s original direction. Thus, all the transverse momentum components of an image refract into the same direction and traverse the cell together, maintaining their phase relation. On exiting the cell, each component returns to its original direction.

an EIT line-width of  $\Gamma = 70$  kHz and transmission at  $\Delta = \pm\Gamma$  of about 1%. In each shot, an image is imprinted on a weak probe pulse ( $2 \mu\text{W mm}^{-2}$ ) and projected onto the entrance facet of the cell. The transmitted probe at the exit facet is recorded with a CCD camera.

A demonstration of image propagation without diffraction is presented in Fig. 2a with an image of the symbol ‘@’. The 100- $\mu\text{m}$  features in the image are significantly distorted after 50 mm of free-space diffraction. On the EIT resonance ( $\Delta = 0$ ), the image covers this distance in 5.75  $\mu\text{s}$ , during which it diffracts and diffuses. However, for  $\Delta = -\Gamma$ , both diffraction and diffusion are clearly suppressed. The corresponding calculations verify that the observed minor spreading for  $\Delta = -\Gamma$  is due to subdiffractive<sup>29</sup> and subdiffusive terms of fourth order in  $k$ . Indeed, the  $k$  spectrum of the image extends beyond the  $k \ll k_0$  region ( $k_0 = 20 \text{ mm}^{-1}$ ), as seen in Fig. 1a (Experiment I). For  $\Delta = +\Gamma$ , and as predicted in equation (2), the image does not diffuse but rather undergoes substantial diffraction, of effectively twice the distance travelled. The presented calculations are done numerically by taking the Fourier transform of the two-dimensional incident field, multiplying by  $\exp[i\chi(\mathbf{k}_\perp)L]$ , and taking the inverse Fourier transform. This computation does not require the paraxial  $k \ll k_0$  approximation and is hereafter denoted as the numerical calculation.

A slow image of a line grating, shown in Fig. 2b, provides a quantitative measurement of the actual diffraction and diffusion. This image has the property that it reappears periodically after propagating a distance of  $L_T = 2a^2/\lambda$ , known as the Talbot self-imaging distance, where  $a$  is the grating period. At  $L_T/2$ , a reciprocal grating is created; the original lines disappear and new lines appear in the originally dark areas. In our experiment, the cell length was  $\sim L_T/4$ , at which the amplitudes of the original and reciprocal gratings are equal, resulting in a grating with a period of  $a/2$ .

The results for  $\Delta = -\Gamma, 0, +\Gamma$  are presented in Fig. 2b. Evidently, the image does not change for  $\Delta = -\Gamma$ , and it is essential to note that, in contrast to a self-imaging effect, the image is maintained throughout its propagation. In the  $\Delta = 0$  image,

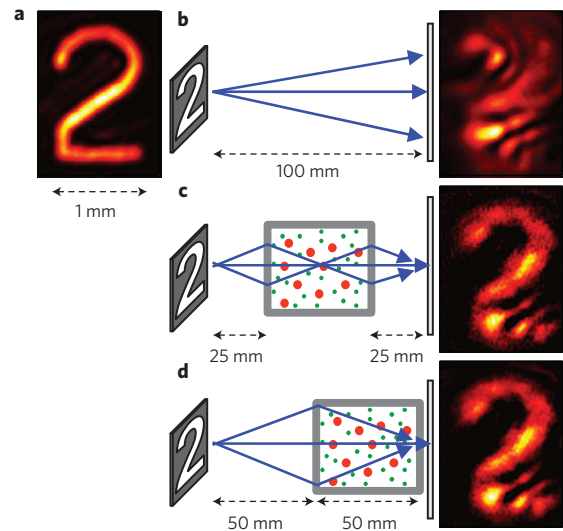


**Figure 4 | A negative-diffraction lens.** **a**, An image of the digit ‘2’ is created at  $u = 25$  mm in front of the entrance facet of the vapour cell, of length  $L = 50$  mm, and the CCD is positioned to image the plane that is  $v = 25$  mm behind the exit facet. **b**, The image is significantly blurred under free-space diffraction of 100 mm. **c,d**, In the negative-diffraction conditions, the 50 mm EIT cell acts as a lens, and the image is made to reappear. To achieve these conditions, the pump power is set to about half the power required for the elimination of diffraction, so that  $\Gamma = 30$  kHz, the group delay is doubled and  $n_{\text{eff}} \cong -1$ . Because the EIT line-width is decreased, the  $k$  filter is narrower ( $k_0 = 13 \text{ mm}^{-1}$ ), making our paraxial approximation less valid and the lens marginally adequate for the purpose. The imperfections in the reconstruction are due to the small  $k_0$ . When entering the cell, the beams refract at an angle opposite to the incident angle, and refract back on exiting, similarly to a negative-refraction-index lens. However, as opposed to the latter, the optical  $k$  vectors do not refract, and it is beam trajectories that are illustrated by the blue lines in the figure. The outcome is independent of the longitudinal position of the cell, as seen by the resemblance of **c** and **d**. Note that this lens is limited to  $|\mathbf{k}_\perp| \ll k_0$  and is therefore not applicable to the evanescent components of the image<sup>30</sup>.

diffusion broadens the lines and erases the grating. For  $\Delta = +\Gamma$ , we observe double diffraction, with the reciprocal grating dominating the original, in correspondence to  $L_T/2$ . To quantify the amount of diffraction, we measure the intensities at the positions of the original and reciprocal gratings,  $\langle I_o \rangle$  and  $\langle I_n \rangle$  respectively, and define the contrast  $C = (\langle I_o \rangle - \langle I_n \rangle) / (\langle I_o \rangle + \langle I_n \rangle)$ , shown in Fig. 2b.  $C = 1$  ( $-1$ ) at integer (half-integer) Talbot distances, and  $C = 0$  when the original and reciprocal gratings are comparable. The maximum value of  $C$  is obtained at  $\Delta = -\Gamma$  and is about 0.85. Notice that  $C = 0$  also when the gratings are indistinguishable owing to diffusion, and quantitative indicators that separate the diffusion and diffraction effects are given in the Supplementary Information.

In addition to the magnitude of diffraction, we can use the atomic-motion mechanism to control the diffraction directionality. By setting a small angle  $\theta_{\text{pump}}$  between the pump and the  $z$  axis, as illustrated in Fig. 3a, we superimpose a transverse phase grating,  $\exp(ixq\theta_{\text{pump}})$ , on the pump–probe interference<sup>5</sup>, replacing  $Dk^2$  in equation (1) with  $D(\mathbf{k}_\perp - q\theta_{\text{pump}}\hat{\mathbf{x}})^2$  (see Supplementary Equation S8). For  $\Delta = \pm\Gamma$  and  $\theta_{\text{pump}} \ll (k_0/q)$ , a term proportional to  $\pm \mathbf{k}_\perp \cdot \hat{\mathbf{x}}\theta_{\text{pump}}$ , which inflicts a directional deflection on the probe, at an angle  $\theta_{\text{probe}} = \mp(qD/v_g)\theta_{\text{pump}}$ , is added to the dispersion in equation (2). Similarly to the walk-off phenomenon in birefringence crystals, the beam is deflected whereas the carrier wavevector stays parallel to the  $z$  axis (equal-phase surfaces maintain their original orientation). Hence, the beam keeps its original direction on exiting the cell.

We have performed deflection experiments in the conditions for diffraction elimination,  $v_g = Dq$  and  $\Delta = -\Gamma$ . Figure 3b presents the measured  $\theta_{\text{probe}}$  versus the applied  $\theta_{\text{pump}}$ , showing that  $\theta_{\text{probe}} = \theta_{\text{pump}}$  as long as the paraxial approximation holds ( $q\theta_{\text{pump}} \ll k_0$ ). This striking phenomenon, that the probe takes the direction of the pump while in the cell regardless of the incident angle, provides another explanation for the elimination of diffraction. As illustrated in Fig. 3b (inset), all diverging  $k$  components of a focused beam are made to propagate in the axial (pump) direction while maintaining their phase relation, thus detaining the diffractive divergence. Supporting measurements and an analytic derivation are given in Supplementary Information.

Diffraction vanishes when the induced diffraction,  $D/(2v_g)$ , is equal in size and opposite in sign to the free-space diffraction,  $1/(2q)$ . However, if the induced diffraction is strengthened, for example by lowering the group velocity, the overall diffraction will become negative. Such a medium reverses the diffraction of slow images and can undo diffraction that has already taken place. As far as spatial diffraction is concerned, a medium with negative diffraction behaves similarly to a negative-refraction-index medium, within the limits of the paraxial approximation. The effective index is  $n_{\text{eff}} = (1 - qD/v_g)^{-1}$ . When  $v_g = qD/2$ ,  $n_{\text{eff}} = -1$  and the overall diffraction becomes exactly the opposite of free-space diffraction.

A fascinating application of negative-index materials is an unusual lens<sup>13</sup>, demonstrated in Fig. 4. This slab-shaped lens of length  $L$  and  $n_{\text{eff}} = -1$  focuses the radiation coming from any point source, located at a distance  $u < L$ , to a distance  $v$  behind the lens, where  $u + v = L$ . Parallel light rays, however, are not focused and continue in their original directions. Indeed, the images in the experiment are reconstructed by the lens regardless of the distance  $u$ .

As a geometrical effect, paraxial diffraction is manifested through  $k$  dependence of the dispersion curve. The optimal approach to eliminate it is to superimpose dispersion with the same form and the opposite sign that is uniform in real space. An EIT vapour medium with a buffer gas and a uniform pump manifests these properties. The pump provides the anisotropy needed to single out the transverse wavevector, and Dicke narrowing accounts for the quadratic  $k$  dependence. The strength, frequency and orientation of the pump control the magnitude, sign and direction of the resulting diffraction. The possibilities may be further extended by introducing a non-uniform pump. The phase gradient of the pump then acts as a vector potential for the probe, in an effective Schrödinger dynamics of a charged particle. Currently, inherent loss limits the effectiveness of the scheme, for example in terms of resolution. Resolving this limitation by combining linear gain, probably by using more elaborate Raman processes, would clear the way to a vast variety of applications, in microscopy, lithography, switching and more.

Received 15 April 2009; accepted 1 July 2009; published online 2 August 2009

## References

- Camacho, R. M., Broadbent, C. J., Ali-Khan, I. & Howell, J. C. All-optical delay of images using slow light. *Phys. Rev. Lett.* **98**, 043902 (2007).
- Shuker, M., Firstenberg, O., Pugatch, R., Ron, A. & Davidson, N. Storing images in warm atomic vapour. *Phys. Rev. Lett.* **100**, 223601 (2008).
- Harris, S. E. Electromagnetically induced transparency. *Phys. Today* **50**, 36–42 (1997).
- Hau, L. V., Harris, S. E., Dutton, Z. & Behroozi, C. H. Light speed reduction to 17 metres per second in an ultracold atomic gas. *Nature* **397**, 594–598 (1999).
- Firstenberg, O. *et al.* Theory of thermal motion in electromagnetically induced transparency: Diffusion, Doppler, Dicke and Ramsey. *Phys. Rev. A* **77**, 043830 (2008).
- Pugatch, R., Shuker, M., Firstenberg, O., Ron, A. & Davidson, N. Topological stability of stored optical vortices. *Phys. Rev. Lett.* **98**, 203601 (2007).
- Firstenberg, O., Shuker, M., Davidson, N. & Ron, A. Elimination of the diffraction of arbitrary images imprinted on slow light. *Phys. Rev. Lett.* **102**, 043601 (2009).
- Moseley, R. R., Shepherd, S., Fulton, D. J., Sinclair, B. D. & Dunn, M. H. Spatial consequences of electromagnetically induced transparency: Observation of electromagnetically induced focusing. *Phys. Rev. Lett.* **74**, 670–673 (1995).
- Truscott, A. G., Frieze, M. E. J., Heckenberg, N. R. & Rubinsztein-Dunlop, H. Optically written waveguide in an atomic vapour. *Phys. Rev. Lett.* **82**, 1438–1441 (1999).
- Rakesh, K. & Agarwal, G. S. Theory of electromagnetically induced waveguides. *Phys. Rev. A* **61**, 053818 (2000).
- Vengalattore, M. & Prentiss, M. Radial confinement of light in an ultracold anisotropic medium. *Phys. Rev. Lett.* **95**, 243601 (2005).
- Friedler, I., Kurizki, G., Cohen, O. & Segev, M. Spatial Thirring-type solitons via electromagnetically induced transparency. *Opt. Lett.* **30**, 3374–3376 (2005).
- Veselago, V. G. The electrodynamics of substances with simultaneously negative values of  $\epsilon$  and  $\mu$ . *Sov. Phys. Usp.* **10**, 509–514 (1968).
- Boyer, V., McCormick, C. F., Arimondo, E. & Lett, P. D. Ultraslow propagation of matched pulses by four-wave mixing in an atomic vapour. *Phys. Rev. Lett.* **99**, 143601 (2007).
- Marino, A. M., Pooser, R. C., Boyer, V. & Lett, P. D. Tunable delay of Einstein–Podolsky–Rosen entanglement. *Nature* **457**, 859–862 (2009).
- Lukin, M. D. & Imamoglu, A. Controlling photons using electromagnetically induced transparency. *Nature* **413**, 273–276 (2001).
- Xiao, M., Li, Y., Jin, S. & Gea-Banacloche, J. Measurement of dispersive properties of electromagnetically induced transparency in rubidium atoms. *Phys. Rev. Lett.* **74**, 666–669 (1995).
- Kasapi, A., Jain, M., Yin, G. Y. & Harris, S. E. Electromagnetically induced transparency: Propagation dynamics. *Phys. Rev. Lett.* **74**, 2447–2450 (1995).
- Schmidt, O., Wynands, R., Hussein, Z. & Meschede, D. Steep dispersion and group velocity below  $c/3000$  in coherent population trapping. *Phys. Rev. A* **53**, R27–R30 (1996).
- Kash, M. M. *et al.* Ultra-slow group velocity and enhanced nonlinear optical effects in a coherently driven hot atomic gas. *Phys. Rev. Lett.* **82**, 5229–5232 (1999).
- Budker, D., Kimball, D. F., Rochester, S. M. & Yashchuk, V. V. Nonlinear magneto-optics and reduced group velocity of light in atomic vapour with slow ground state relaxation. *Phys. Rev. Lett.* **83**, 1767–1770 (1999).
- Fleischhauer, M. & Lukin, M. D. Dark-state polaritons in electromagnetically induced transparency. *Phys. Rev. Lett.* **84**, 5094–5097 (2000).
- Bolkart, C., Rostohar, D. & Weitz, M. Dark resonances with variable Doppler sensitivity. *Phys. Rev. A* **71**, 043816 (2005).
- Shuker, M. *et al.* Angular dependence of Dicke-narrowed electromagnetically induced transparency resonances. *Phys. Rev. A* **76**, 023813 (2007).
- Taichenachev, A. V. *et al.* Nonlinear-resonance line shapes: Dependence on the transverse intensity distribution of a light beam. *Phys. Rev. A* **69**, 024501 (2004).
- Xiao, Y., Novikova, I., Phillips, D. F. & Walsworth, R. L. Diffusion-induced Ramsey narrowing. *Phys. Rev. Lett.* **96**, 043601 (2006).
- Eisenberg, H. S., Silberberg, Y., Morandotti, R. & Aitchison, J. S. Diffraction management. *Phys. Rev. Lett.* **85**, 1863–1866 (2000).
- Fleischer, J. *et al.* Spatial photonics in nonlinear waveguide arrays. *Opt. Express* **13**, 1780–1796 (2005).
- Staliunas, K. & Herrero, R. Nondiffractive propagation of light in photonic crystals. *Phys. Rev. E* **73**, 016601 (2006).
- Pendry, J. B. Negative refraction makes a perfect lens. *Phys. Rev. Lett.* **85**, 3966–3969 (2000).

## Acknowledgements

We thank D. Yankelev for assistance with the experiments and Yoav Erlich for technical support. We thank R. Pugatch for discussions and suggestions.

## Author contributions

O.F. conceived the idea with significant input from A.R. and N.D. O.F. and A.R. carried out the theoretical modelling. The experiment was conducted by O.F. with the assistance of P.L. and M.S., and all authors contributed to the data analysis. The paper was written by O.F., M.S. and N.D.

## Additional information

Supplementary information accompanies this paper on [www.nature.com/naturephysics](http://www.nature.com/naturephysics). Reprints and permissions information is available online at <http://npg.nature.com/reprintsandpermissions>. Correspondence and requests for materials should be addressed to O.F.